Synthesis and *in vivo* Behaviour of an Exendin-4-Based MRI Probe Capable of β-cell-dependent Contrast Enhancement in the Pancreas

Thomas J. Clough[a], **Nicoleta Baxan**[b], **Emma J. Coakley**[a], **Charlotte Rivas**[a], **Lan Zhao**[b,c], **Aida Martinez-Sanchez**[d], **Guy A. Rutter**[d,e], **Nicholas J. Long**[a]

[a]Department of Chemistry, Molecular Sciences Research Hub, Imperial College London, White City Campus, Wood Lane, London, W12 0BZ, UK

[b]Biological Imaging Centre, Faculty of Medicine, Hammersmith Hospital, Du Cane Road, London, W12 0NN, UK

[c]National Heart and Lung Institute, Faculty of Medicine, Hammersmith Hospital, Du Cane Road, London, W12 0NN, UK

[d]Section of Cell Biology and Functional Genomics, Department of Metabolism, Digestion and Reproduction, Faculty of Medicine, Hammersmith Hospital, Du Cane Road, London, W12 0NN, UK

[e]Lee Kong Chain School of Medicine, Nan Yang Technological University, 11 Mandalay Road, 308232 Singapore

Abstract

Global rates of diabetes mellitus are increasing, and treatment of the disease consumes a growing proportion of healthcare spending across the world. Pancreatic β-cells, responsible for insulin production, decline in mass in Type 1 and, to a more limited degree, in Type 2 diabetes. However, the extent and rate of loss in both diseases differs between patients resulting in the need for the development of novel diagnostic tools, which could quantitatively assess changes in mass of β-cells over time and potentially lead to earlier diagnosis and improved treatments. Exendin-4, a potent analogue of glucagon-like-peptide 1 (GLP-1), binds to the receptor GLP-1R, whose expression is enriched in β-cells. GLP-1R has thus been used in the past as a means of targeting probes for a wide variety of imaging modalities to the endocrine pancreas. However, exendin-4 conjugates designed specifically for MRI contrast agents are an under-explored area. In the present work, the synthesis and characterization of an exendin-4-dota(ga)-Gd(III) complex, **GdEx,** is reported, along with its *in vivo* behaviour in healthy and in β-cell-depleted C57BL/6J mice. Compared to the ubiquitous probe, [Gd(dota)]⁻, **GdEx** shows selective uptake by the pancreas with a marked decrease in accumulation observed after the loss of β-cells elicited by deleting the microRNA processing enzyme, DICER. These results open up pathways towards the development of other targeted MRI contrast agents based on similar chemistry methodology.

Conflicts of interest
There are no conflicts to declare.

Introduction

In 2008 there were an estimated 347 million people in the world living with diabetes mellitus.[1] According to the WHO, in 2014 that number had already risen to approximately 420 million and is expected to rise to more than 600 million by 2040[2,3]. What had once been regarded as a disease of the Western world, associated with poor diet, sedentary lifestyles and obesity, is now considered a pandemic[4]. Diabetes is characterised by an inability to moderate the body's glucose levels through insufficient insulin production, or by desensitisation or resistance to insulin.

In non-diabetic subjects, insulin is released in response to elevated blood glucose levels[5], triggering the conversion of glucose into glycogen for storage within the muscles and liver, as well as the synthesis and storage of triglycerides in adipose tissue[6]. In diabetes, hyperglycaemia is associated acutely with thirst and the frequent need for urination. If left untreated, chronic debilitating conditions such as blindness, kidney failure and tissue necrosis can develop. The pathway that leads to type 1 diabetes (T1D) results from an autoimmune response that provokes the body's immune cells to attack of β-cells, the insulin production centre, leading to their destruction[7,8]. Type 2 diabetes (T2D) is characterised by insulin resistance and involves both β-cell dysfunction and loss[9],though the extent of the latter is thought to be more limited[10]. The production of non-esterified fatty acids, glycerol, hormones and cytokines from adipose tissues are contributing factors in this insulin resistance,[11] which accompanies the dysfunction of pancreatic β-cells.

Gadolinium(III) complexes are well-known as MRI contrast agents[12–17]. Despite an urgent need to better understand the contributions to disease etiopathology of β-cell loss *vs.* impaired function, and more than three decades of research, there is still a lack of tractable gadolinium-based contrast agents (GBCAs) targeted to pancreatic β-cells, e.g. through incorporation of peptides or small molecules[18], and capable of following β-cell mass *in vivo*. As zinc(II) ions are strongly enriched in pancreatic β-cells[19] it is conceivable that the incorporation of a zinc-binding group could aid in the magnetic resonance imaging of these elusive cells, which make up only ~ 2% of pancreas volume[8,20–22]. This strategy has also been put to use by others in the field, with a particular focus on imaging of glucose-mediated insulin secretion utilising a GBCA which incorporates a zinc sensing moiety[23–26]. Notable amongst these is the synthesis of the agent [Gd(dota-diBPEN)] by Esqueda *et al.* in 2009, which employs two zinc-binding moieties and binds to Zn^{2+} selectively and with a high affinity[23]. The resulting ternary complex then binds to serum albumin proteins, resulting in a 3-fold increase in relaxivity[23,24,26]. The free ligand does not interaction with serum proteins, and this relaxivity increase in the presence of zinc(II) ions has been utilised to give a qualitative assessment of β-cell functionality and detection of pancreatic tissue expansion through detection of the co-release of zinc(II) ions alongside insulin[24–26]. The compound's large relaxivity increase and high affinity for Zn^{2+} could enable valuable insight into the physiological changes associated with diabetes development *in vivo* and could allow the use of the probe at lower concentrations than other clinically used GBCAs. However, probes based on this approach developed within our group have met with only limited success[8], indicating that other β-cell-enriched targets need to be identified and deployed. Furthermore, the targeting ability of these compounds arises exclusively from their incorporation of a

zinc-sensing moiety. The addition of a specific targeting group, such as a peptide, may aid the delivery of MRI contrast agents to β-cells and result in enhanced pancreatic contrast.

Exendin-4 and GLP-1

Glucagon-like peptide 1 receptors (GLP-1R), members of the class B G-protein coupled receptor family[27], are strongly enriched in pancreatic β-cells[28–30], but are barely detectable in other islet neuroendocrine cells[31]. Correspondingly, GLP-1R agonists are effective therapeutics for the treatment of type 2 diabetes. GLP-1 acts as an incretin, being released from the gut during food transit and contributing to the lowering in blood glucose levels[32]. However, as it is a metabolically unstable endogenous ligand, GLP-1 cannot readily be used therapeutically. Exendin-4 is a 39 amino acid-long peptide, first isolated from the venom of the Gila monster, which shares 53% of homology with GLP-1 and has been used as an effective agent for the treatment of diabetes[33]. Additionally, it has been approved for clinical use in drugs such as exenatide (a synthetic version of exendin-4) and lixisenatide[20,34]. When taken after food, exendin-4 increases the release of insulin and has been shown to have a more than 10-fold longer blood plasma half-life than GLP-1, making it a more potent insulinotropic agent[35]. Exendin-4 has also been shown to have an anti-apoptotic function on β-cells: treatment of mouse pancreas cells with exendin-4 has been observed to result in an increase in β-cell mass, alongside a decrease in the number of apoptotic cells[36,37].

Exendin-4 has been conjugated with therapeutic and imaging agents to act as a targeting moiety for pancreatic β-cells[3,20,38–48]. In 2012 Kiesewetter *et al.* [41] synthesised and evaluated a series of ^{18}F-labelled exendin-4 analogues for their GLP-1R affinity in an INS-1 xenograph tumour model. Evaluating the cellular uptake, stability and specificity of the Cys^{40} and Cys0 isomers, these authors found the C-terminal isomer ([^{18}F]FBEM-[Cys^{40}]-exendin-4) to have a much higher uptake and affinity for the INS-1 tumour cells and therefore GLP-1R. A number of other probes utilising conjugation to ^{18}F for PET imaging have been reported in the literature, some of which are capable of dual-modal imaging[20,28,49,50]

In 2013 Selvaraju *et al.*[42] demonstrated the use of a ^{68}Ga-labelled H_4dota analogue ^{68}Ga-do3a-VS-Cys^{40}-exendin-4 for quantification of GLP-1R in the pancreas. They compared the uptake of the probe in both diabetic and healthy rats and found that pre-administration of exendin-4 prior to injection with the labelled probe resulted in a decrease in signal upon injection of the ^{68}Ga-labelled probe. This competitive binding investigation indicated that the probe itself was binding to GLP-1R, and therefore that the affinity of exendin-4 for GLP-1R remains unaffected by synthetic modifications to introduce metal chelating moieties. The uptake of the probe in diabetic rats was significantly reduced compared with that of healthy rats, providing a way of monitoring the reduction of GLP-1R in diabetic subjects through ^{68}Ga radioimaging. Further success in radioimaging techniques has been had with ^{68}Ga-do3a-exendin-4, which has shown a difference in tracer uptake in the pancreas before and after the administration of streptozotocin to induce β-cell destruction[20,42]. The probe showed a reduced level of uptake in both rats and non-human primates which had been subjected to streptozotocin[42].

Quantification of β-cell mass through the use of single photon emission computed tomography (SPECT) imaging probes based on exendin derivatives has been widely reported on throughout the literature[3,20,43,44,47,48,51–53]. Gotthardt *et al.* have established that a decrease in β-cell mass can be determined through quantitative analysis of SPECT images[43,44]. Additionally, the group has recorded that there is a decrease in GLP-1R expression during periods of hyperglycaemia, which corresponds with a reduced uptake of probes based on exendin during periods of elevated blood glucose levels[43,44]. One further innovative use of radiolabelled exendin-based probes utilised by Eter *et al.* has been to monitor islet graft volume through β-cell mass quantification, signalling another potential use of these compounds and their developing role in both the diagnosis and treatment of diabetes[51].

An additional example of an exendin-4 conjugate is that of Lys^{40}(Ahx-HYNIC-^{99m}Tc/EDDA)NH_2-exendin-4. This probe, developed for SPECT imaging by Wild *et al.* [45]and Sowa-Staszczak *et al.*[46], has been studied in humans and has exhibited localised insulinoma uptake in patients where other imaging probes and modalities failed to locate biochemically proven tumours[20,54–56]. Additionally, the probe has been used for the visualisation of thyroid tumours[20,45,56]. Several examples of SPECT imaging agents based on chelators for ^{111}In have also been reported, notably those from Gotthardt *et al.*, Reiner *et al.* and Kimura *et al.*, which have shown specific binding to receptor tissues expressing GLP-1R[3,20,47,48].

More recently, Cys^{40}-exendin-4 has been used with 1, 4, 7-triazacyclononane-1,4,7-triacetic acid, (NOTA) conjugates in ^{68}Ga imaging for the detection of localised insulinomas[40]. The application of exendin-4 for radio-imaging pancreatic insulinomas originating from β-cells has proven successful through both PET and SPECT, yet fruitful targeting and visualisation utilising magnetic resonance techniques is less well established. Some prior work in this area exists, usually generalised to the conjugation of exendin-4 to nanoparticles. Functionalisation of iron oxide nanoparticles with exendin-4 has been achieved by both Wang *et al.* and Vinet *et al.* for the imaging of pancreatic β-cells *via* GLP-1R targeting[38,39]. Both groups reported enhanced contrast in wild-type mice compared to the diabetic models. Wang *et al.* have also incorporated a cyanine fluorophore Cy5.5 into their scaffold to achieve dual-modal imaging from which they were able to identify the accumulation of the probe in β-cells through *ex vivo* histology analysis. Figure 1 shows some examples of recently reported exendin-4 conjugates.

Whilst radiochemical techniques such as PET and SPECT offer high sensitivity, MRI offers much greater spatial resolution and allows the avoidance of ionising radiation and the time constraints involved in radiochemical syntheses[57]. Thus, typical syntheses of radionuclide-carrying probes - which must be done immediately before use in a given patient - may require 2-4 hours, greatly increasing the overall length, and cost, of the procedure. These limitations argue for the development of simpler MRI-based strategies. All existing clinically-approved MRI contrast agents are based on gadolinium(III) complexes of polyaminocarboxylate ligands, which provide a ready scaffold for functionalisation[13,58]. Previous work in our group has dealt with dual-modal fluorescent-MRI contrast agents for pancreatic β-cells, which exhibited selective retention in the pancreas over [Gd(dota)]- due to the zinc-sensing moiety which was included[8]. We hypothesised that the introduction of a

targeting group would help us build on this work and develop probes with greater avidity and selectivity for the β-cell.

Results and Discussion

Probe Synthesis

The synthesis of the MRI contrast agent **GdEx** was achieved in two straightforward steps. The first of these was a bioconjugation step, resulting in the free ligand 1. This step utilised H_4dota(ga)-maleimide, a modified ligand based on H_4dota with the incorporation of a glutamic acid (ga) side arm allowing functionalisation, and a synthetic variant of exendin-4, with an additional cysteine residue added at the C-terminus (HGEGTFTSDLSKQMEEEAVRLFIEWLKNGGPSSGAPPPS-[C]), both of which are commercially available. Dissolution of the peptide in phosphate-buffered saline (PBS) at pH 7.4, followed by addition of a slight excess (1.1. equivalents) of the maleimide gave a solution which was incubated at 3 °C. After 24 hours, formation of compound 1 could be confirmed by LCMS, which indicated quantitative conversion. After lyophilisation, the resulting solid was readily dissolved in water and $GdCl_3.6H_2O$ added portion-wise to the reaction mixture over 24 to 72 hours, whilst maintaining a pH of 5.5. Once LCMS indicated complete conversion, the reaction mixture was again lyophilised before being purified by automated reverse-phase flash chromatography to give **GdEx** in yields of around 50% across the two steps. This short synthetic pathway limits loss of the valuable synthetic peptide and enabled sufficient quantities of probe for *in vivo* work to be produced in short periods of time. The complete synthetic route to **GdEx** is shown in Scheme 1.

The current 'gold standard' for GBCAs is [Gd(dota)]⁻. This macrocyclic species was one of the first developed probes which went on to be clinically approved. The relaxivity of **GdEx** was calculated to be 6.1 mM^{-1} s^{-1}, greater than that of [Gd(dota)]⁻ which is 4.3 mM^{-1} s^{-1} at 400 MHz[59], an increase likely attributed to the increased molecular weight and rotational correlation time of **GdEx** [60]. Despite its prevalence today, [Gd(dota)]⁻ lacks any targeting moiety, rendering imaging of specific biological tissues challenging and resulting in the need for administration of larger quantities of contrast agent in order to obtain meaningful contrast enhancement in images of specific organs or tissues. This is of concern in recent years due to the discovery of the link between GBCA administration and nephritic systemic fibrosis (NSF)[61–66]. Whilst the concerns around the use of GBCAs and NSF have primarily been associated with the use of gadolinium(III) complexes of acyclic ligands, several organisations are concerned with potential excess use of GBCAs in patients[67], and introducing a targeting moiety may help lower the quantity required to achieve sufficient contrast in the organ of interest. It was decided to synthesise [Gd(dota)]⁻ and compare its biodistribution *in vivo* to **GdEx** to examine whether the use of exendin-4 resulted in pancreas-specific contrast enhancement.

in vivo Studies of GdEx

GdEx accumulates in pancreas: In order to assess the specificity, efficacy and targeting ability of **GdEx** *in vivo*, the probe (1.12 μmol/mouse) was injected into five 12-14 week-old

male wild-type C57BL/6J mice. Each mouse was scanned for a period of up to 54 minutes after injection.

The impact of **GdEx** on the CNR (contrast to noise ratio) of pancreas was compared with that of [Gd(dota)]$^-$ [8]. With Gd(dota)]$^-$ a large increase in CNR of up to 30% was observed at 18 minutes followed by a smooth gradual decay plateauing out to baseline values at 54 minutes (Figure 2A), where a CNR value of 100% is the baseline value. In contrast, changes in CNR after **GdEx** injection showed an overall stronger enhancement peaking at 73% above baseline at 18-21 minutes followed by slower decline with values remaining significantly higher compared to [Gd(dota)]$^-$, despite the same dosage of probe being used, (50% increase relative to the baseline) up to 54 minutes (Figure 2B, left). The consistent maximal CNR peak observed at 18-21 minutes may coincide with the timing of full accumulation of the probes in blood plasma followed by either (1) full clearance of non-targeted [Gd(dota)]$^-$ or (2) retention in the pancreas likely reflecting localisation to the β-cell. The CNR enhancement of the **GdEx** relative to [Gd(dota)]$^-$ was consistently higher over the entire time course as confirmed by the AUC analysis (Figure 2B, right). Previous work in our group has shown increased retention time in the pancreas of wild-type Balb/C mice of a dual-modal MRI-fluorescence imaging probe, **Gd1**, over that observed with [Gd(dota)]$^{-8}$. The specificity of this probe was attributed to its zinc-sensing moiety, as discussed above, resulting in an increase in CNR of around 7% over that achieved with [Gd(dota)]$^{-8}$.The results presented here indicate that the exendin-4 targeting moiety in **GdEx**, rather than the general presence of the paramagnetic Gd^{3+} ion is responsible for pancreatic contrast enhancement and confers **GdEx** improved targeted uptake and retention into the β-cells within the pancreas.

GdEx accumulation depends on β-cell mass:

To determine whether GdEx can be used as a contrast agent to detect decreased β-cell mass in vivo we took advantage of a mouse strain with tamoxifen-inducible, β-cell-specific, Dicer deletion (βDicer-null) that we have previously characterized in detail[68]. DICER is an RNAseIII enzyme indispensable for miRNA production and thus essential for β-cell development and function[68,69]. Four weeks after tamoxifen injections, βDicer-null mice present with exceptional hyperglycaemia and glucose intolerance and a sharp (~80%) reduction in β-cell mass as measured post-mortem by insulin immunostaining. The latter reflects increased β-cell apoptosis and de-differentiation[68]. To assess whether **GdEx** detects this decrease in β-cell mass *in vivo*, βDicer-null (Dicerfl/fl, Cre-ER positive) and littermate control (βDicer-control, Dicerfl/fl, Cre-ER negative) mice were injected with tamoxifen and, four weeks later, scanned using **GdEx** as contrast agent. As expected, βDicer-null mice were strongly hyperglycaemic at the time of MRI (Supporting Figure 1). As previously observed in wild-type mice, a maximal peak of CNR enhancement was detected at 18-21 minutes in both βDicer-control and -KO mice (Figure 2C). Nevertheless, there was a distinctive trend of signal decrease over time in βDicer-null compared to controls with significance reached chiefly at later time-points, from 21 minutes onwards (Figure 2C). Consistently, AUC analysis showed no differences in CNR between βDicer-control and βDicer-null mice up to 21 min. which suggests similar uptake of **GdEx** in both groups whereas AUC of CNR was much lower in the βDicer-null mice from 21 to 54 minutes (~1.8-fold, p=0.08). These results

suggest a weaker retention of the probe in the pancreas (only 15-20% CNR increase from baseline) of βDicer-null mice and a complete **GdEx** wash out by 54 minutes. It is worth noting that the level of CNR enhancement in βDicer-control animals (Figure 2B) was consistently lower than in wild-type animals (Figure 2A). Even though this was initially surprising taking into account that these animals share the same genetic background (C57BL/6J), age and sex, it was not totally unexpected given that βDicer-control mice (as well as, importantly, βDicer-null mice) were administered tamoxifen dissolved in a high volume (100 μl per day, for 5 days, per animal) of corn-oil intraperitoneally. It is thus likely that the tamoxifen and/or the noticeable presence of corn oil around the organs at the time of imaging resulted in a non-specific reduction of CNR.

Summary of *in vivo* data

Although the βDicer-null mouse may be considered a fairly extreme model of the loss of β-cell mass in the development of diabetes mellitus, **GdEx** convincingly demonstrates that a decline in cell mass may be quantitatively monitored through reduced pancreatic uptake of a GBCA targeted to β-cells *via* the GLP-1R receptor. Further refinement of our model may be possible through *in vivo* analysis of βDicer-null mice at a series of time points throughout the evolution of the disease following gene deletion – this would enable assessment of the probe in the face of subtle changes in the mass of β-cells, which may occur early in the development of T1D or T2D. MRI offers significantly improved resolution over rival PET and SPECT techniques and avoids the need to carry out rapid radiochemical synthesis and purification. Although large quantities of the probe were required, a necessary factor given the lower sensitivity of MRI compared to other imaging techniques, no undue hyperglycaemia was observed in any of the mice, suggesting that the amount of GLP-1R ligand utilised did not result in any undesired effects.

Experimental Details

Synthetic Chemistry: Solvents and reagents were of Analar or reagent grade and were purchased from Sigma-Aldrich Chemical Co., VWR International or Macrocyclics and used without further purification. Cys[40]-exendin-4 was purchased from Peptide Synthetics and was also used without further purification. Mass spectra were recorded on an Aglient 6200 TOF LC-MS instrument. Automated flash chromatography was performed using a Biotage Isolera Four unit and a 12 G KP-SIL C18 cartridge.
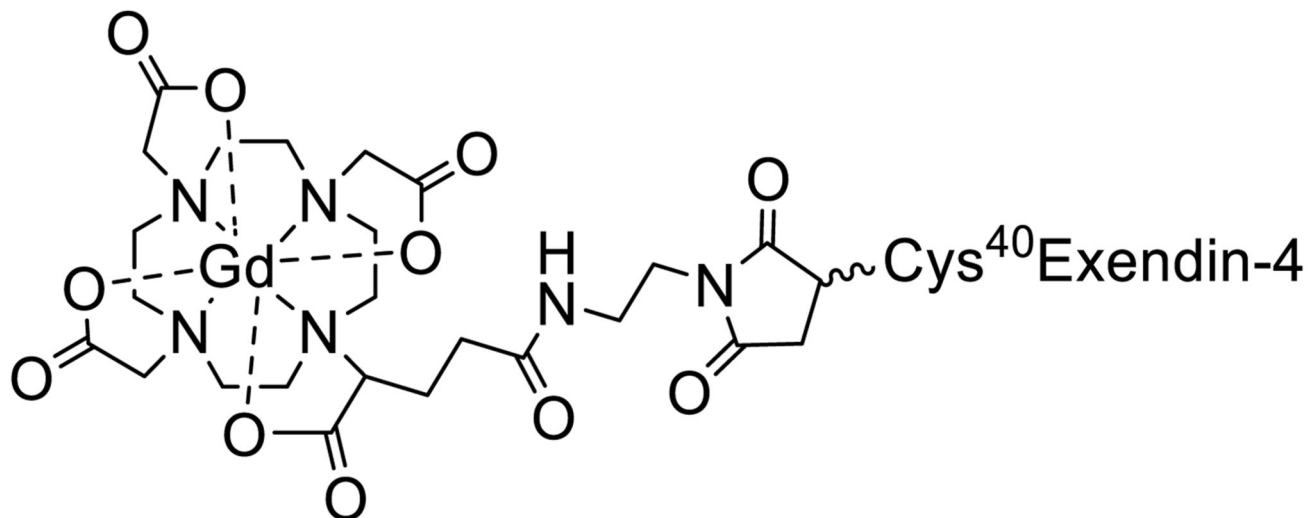
Gd-dota(ga)-maleimide-Cys40Exendin-4, GdEx,: **Cys^{40}Exendin-4** (0.040 g, 9.39 μmol) was dissolved in PBS (pH 7.4, 3.5 mL). H$_4$dota(ga)-maleimide (0.007 g, 11.53 μmol) was added and the solution incubated at 3 °C. After 24 hours, the reaction mixture was lyophilised to leave a white solid. This solid was re-dissolved in H$_2$O (5 mL) and GdCl$_3$·6H$_2$O (0.009 g, 25.29 μmol) was added, and the pH brought to 6 by addition of NaOH (aq., 0.1 M) before the reaction mixture was left to stir at room temperature. After 19 hours, LCMS indicated partial complexation, so an additional portion of GdCl$_3$•6H$_2$O (0.013 g, 34.97 μmol) was added, bringing the pH to 5. The pH was readjusted to 6 by addition of NaOH (aq., 0.1 M) and the reaction mixture left to stir at room temperature. After a further 22 hours, LCMS indicated complete conversion of starting material and the reaction mixture was lyophilised, leaving a white solid. Automated flash chromatography (C$_{18}$ cartridge, 99.9% H$_2$O/0.1% TFA to 99.9% MeCN/0.1% TFA) gave **GdEx** as a white solid (0.022 g, 4.42 μmol, 47%).

ESI MS (ES+) *m/z* for C$_{212}$H$_{320}$GdN$_{56}$O$_{73}$S$_2$:[M]$^{5+}$ - calculated = 1008, found = 1009.37, [M]$^{4+}$ - calculated = 1260.00, found = 1261.35 [M]$^{3+}$ - calculated = 1680.00, found = 1679.74.

Mouse maintenance: Male C57BL/6J mice were purchased from Charles River Laboratories (UK). βDicer-null (βDicer-null mice: Dicer$^{fl/fl}$, Cre-ER positive, heterozygous) and littermate controls βDicer-control (βDicer-control mice: Dicer$^{fl/fl}$, Cre-ER negative) were generated as previously described[68]. 2-5 animals were housed in ventilated cages with a 12-hour light/dark cycle and free access to standard chow diet in a pathogen-free facility (Imperial College Central Biomedical Service). When indicated, 8-10 week-old animals were injected intraperitoneally with five doses of 2 mg tamoxifen (Sigma-Aldrich).

All *in vivo* procedures were approved by the UK Home Office Animals Scientific Procedures Act, 2986 (HO Licence PPL PA03F7F0F). Glucose levels were measured after imaging using an Accucheck Performa nano from blood samples from the tail.

Magnetic Resonance Imaging: Mice were first anaesthetized in an anaesthesia box with 1-5% vol isofluorane in O_2. A tail-vein catheter was placed under anaesthesia (~2% vol) and maintained in the animals throughout the scan to allow administration of the probe and ensure the MR images were acquired at the same location before and after contrast administration.

All MRI scans were conducted on a pre-clinical 9.4 T scanner (94/20 USR Bruker BioSpec, Ettlingen, Germany) equipped with a 40 mm quadrature mouse body transceiver. Mice were positioned prone in a dedicated mouse bed and maintained under anaesthesia. Respiration and body temperature were continuously monitored through the entire imaging session (SA Instruments, Stony Brook, NY, USA). Body temperature was maintained at 36.5° by a circulating warm water heat mat. Data were acquired with Paravision 6.0.1 (Bruker, BioSpin). As a standard, the coronal plane was chosen, and the adjacent organs (kidney, spleen) were used as essential landmarks. T_2 weighted images were initially obtained to locate the pancreas since they provided the best contrast between the pancreas and adjacent organs. T_1 images of same geometry as the T_2 weighted were used further to assess the **GdEx**/[Gd(dota)]$^{-|}$ behaviour *in vivo* due to the specific impact of **GdEx**/[Gd(dota)]$^-$ to shorten the T_1 relaxation time generating brighter T_1 contrast. The peri-pancreatic fat within areas of pancreatic parenchyma was reduced by using a fat saturation T_1 protocol. All scans were respiratory triggered to avoid motion artefacts coming from breeding.

Dynamic T_1 weighted images (TR/TE = 160/2.360 ms, voxel size (140 x 140 x 600) μm^3) were acquired every 3 minutes to assess the **GdEx** kinetic uptake, retention and washout from the pancreas. Specifically, after 4 baseline images, **GdEx**/[Gd(dota)]-(1.12 μmol/ animal in 150μl of saline) was delivered intravenously and a series of T_1 images of the same acquisition parameters and geometry were acquired up to 54 minutes post-injection.

MR Data Analysis: To keep consistency, the pancreas was outlined in each T_1 weighted image primarily based on its anatomical location relative to neighbouring organs. Namely, the spleen and superior aspect of the left kidney were used to identify the tail of the pancreas. At every time series, the mean intensity of outlined pixels of the pancreas and of the spleen were computed along with the standard deviation of image noise. The signal intensity difference between pancreas and spleen was then scaled to the standard deviation of image noise. The resulting parameter was referred to as contrast to noise ratio (CNR) and the results were presented as percentage of CNR change compared to the baseline values.

Statistical analysis was performed using GraphPad Prism 7.0. Data are presented as mean $\pm$ S.E.M. To better visualize the signal distribution of each time course, smoothing was performed by averaging two values on each side and using a second order polynomial smoothing[70]. Two-way ANOVA with Fisher least significant difference (LSD) test was used for time course analysis with each individual time point analysed respectively. Unpaired Student's t-test was performed for area under the curve (AUC) analysis.

Conclusions and Outlook

A straightforward, replicable synthetic route towards a novel MRI contrast agent incorporating a dota(ga)-Gd(III)chelate and the peptide exendin-4 has been developed, producing the novel probe **GdEx** at respectable yields. Although fairly large quantities must be injected, which could result in cost issues during any translation to the clinic, the probe shows significant contrast enhancement, up to 70% above baseline, in the pancreas of healthy mice, indicative of successful targeting of the GLP-1R receptor, highly expressed in pancreatic β-cells. When comparing the results of **GdEx** to scans with the current gold standard MR probe, [Gd(dota)]⁻, **GdEx** was shown to provide greater contrast enhancement in the pancreas with CNR values around 40% higher. This is indicative of successful targeting of pancreatic β-cells through the inclusion of exendin-4 and confirms that the biological properties of the peptide are not interfered with by its incorporation into a bifunctional chelator.

Importantly, we also show here that the retention of **GdEx** in the pancreas of βDicer-null mice is notably reduced in comparison with βDicer-control animals. βDicer-null mice are characterized by a strong reduction in β-cell mass and therefore our experiments provide proof-of-principle on the suitability of **GdEx** to detect β-cell mass deterioration *in vivo*. Even though it is widely accepted that T1D develops as a consequence of an important loss in β-cell numbers following auto-immune destruction, the contribution of β-cell loss to the development of T2D remains contested[71]. This has been largely due to the limited number of techniques available to reliably measure β-cell mass in the living organism. As a stable, non-toxic probe, **GdEx** will be a potent tool for the scientific community to measure β-cell mass *in vivo* and to settle this debate in research models. However, a large dosage of the probe is required for successful pancreatic imaging, especially when compared to alternative imaging modalities. As such, we propose that our work acts as a proof of principle: that it is possible to develop MR contrast agents capable of contrast enhancement in the pancreas and that this paves the way for future targeted contrast agents which could allow β-cell quantification whilst avoiding patient exposure to ionising radiation and the associated synthetic challenges of radiochemistry. We also hope that **GdEx** will represent a base for future probes that will ultimately be used for the early diagnosis and monitoring of diabetes in the clinic, ideally by optimising these for lower dosage.

Future work in this area will focus on measurement of β-cell functionality through quantification of Zn^{2+} ion levels. The inclusion of a zinc-sensing moiety in a targeted Gd(III)-do3a conjugate would theoretically enable quantification of Zn^{2+} ions in pancreatic β-cells through ratiometric changes in probe relaxivity, allowing any decline in cell mass or functionality to be determined. Additionally, there is the potential to study the probe's biodistribution in other animal models. Future work could also involve the utilization of this bioconjugation strategy with chelators for other metals involved in MRI contrast agents, such as manganese(II), or to other ligands for gadolinium(III). Alternatively, other potent, stable agonists of GLP-1R could be explored in order to further develop GBCAs targeted to the pancreas thus aiding the quantification of β-cell mass in diabetic and prediabetic patients.

Acknowledgements

Notes and References

Supplementary figures include characterisation data of the free ligand, compound **1** and the probe **GdEx**. In addition, there is further information on the β-cell-specific deletion of DICER (βDicer-null).

1. Danaei G, Finucane MM, Lu Y, Singh GM, Cowan MJ, Paciorek CJ, Lin JK, Farzadfar F, Khang YH, Stevens GA, Rao M, et al. Lancet. 2011; 378:31–40. [PubMed: 21705069]

2. Ezzati M. Lancet. 2016; 387:1513–1530. [PubMed: 27061677]

3. Kimura H, Fujita N, Kanbe K, Matsuda H, Watanabe H, Arimitsu K, Fujimoto H, Hamamatsu K, Yagi Y, Ono M, Inagaki N, et al. Bioorg Med Chem. 2017; 25:5772–5778. [PubMed: 28927802]

4. Hu FB. Diabetes Care. 2011; 34:1249–1257. [PubMed: 21617109]

5. Rutter GA, Pullen TJ, Hodson DJ, Martinez-Sanchez A. Biochem J. 2015; 466:203–218. [PubMed: 25697093]

6. Ferrannini E, DeFronzo RA. International Textbook of Diabetes Mellitus. 2015:211–233.

7. Pugliese A. International Textbook of Diabetes Mellitus. 2015:442–453.

8. Stasiuk GJ, Minuzzi F, Sae-Heng M, Rivas C, Juretschke H, Piemonti L, Allegrini PR, Laurent D, Duckworth AR, Beeby A, Rutter GA, Long NJ. Chem – A Eur J. 2015; 21:5023–5033.

9. Butler AE, Janson J, Bonner-Weir S, Ritzel R, Rizza RA, Butler PC. Diabetes. 2003; 52:102–110. [PubMed: 12502499]

10. Rahier J, Guiot Y, Goebbels RM, Sempoux C, Henquin J-C. Diabetes, Obes Metab. 2008; 10:32–42. [PubMed: 18834431]

11. Mukherjee B, Hossain CM, Mondai L, Paul P, Ghosh MK. Lipid Insights. 2013; 6:1–11. [PubMed: 25278764]

12. European Medicines Agency. Assessment report for Gadolinium-containing contrast agents. Vol. 44. London, U.K: 2010.

13. Faulkner, S, Blackburn, OA. The Chemistry of Molecular Imaging. Long, N, Wong, W-T, editors. John Wiley & Sons; Hoboken, U.S.A: 2015. 179–197.

14. Sherry AD, Caravan P, Lenkinski RE. J Magn Reson Imaging. 2009; 30:1240–1248. [PubMed: 19938036]

15. Caravan P, Ellison JJ, McMurry TJ, Lauffer RB. Chem Rev. 1999; 99:2293–2352. [PubMed: 11749483]

16. Pierre VC, Allen MJ, Caravan P. J Biol Inorg Chem. 2014; 19:127–131. [PubMed: 24414380]

17. Caravan P. Chem Soc Rev. 2006; 35:512–523. [PubMed: 16729145]

18. Laurent D, Vinet L, Lamprianou S, Daval M, Filhoulaud G, Ktorza A, Wang H, Sewing S, Juretschke H-P, Glombik H, Meda P, Boisgard R, Nguyen DL, Stasiuk GJ, Long NJ, Montet X, Hecht P, Kramer W, Rutter GA, Heckscher-Sorensen J. Diabetes, Obes Metab. 2016; 18:6–15. [PubMed: 26228188]

19. Scott DA, Fisher AM. J Clin Invest. 1938; 17:725–728. [PubMed: 16694619]

20. Jodal A, Schibli R, Béhé M. Eur J Nucl Med Mol Imaging. 2017; 44:712–727. [PubMed: 28025655]

21. Hernandez R, Graves SA, Gregg T, VanDeusen HR, Fenske RJ, Wienkes HN, Engl CG, Valdovinos HF, Jeffery JJ, Barnhart TE, Severin GW, Nickles RJ, Kimple ME, Merrins MJ, Cai W. Diabetes. 2017; 66:2163–2174. [PubMed: 28515126]

22. Kim MJ, Yu JH, Oh MH, Nam YS, Lee DY. J Ind Eng Chem. 2017; 45:404–411.

23. Esqueda AC, López JA, Andreu-de-Riquer G, Alvarado-Monzón JC, Ratnakar J, M AJ, Lubag, Sherry AD, DeLeón-Rodríguez LM. J Am Chem Soc. 2009; 131:11387. [PubMed: 19630391]

24. Martins AF, Clavijo Jordan V, Bochner F, Chirayil S, Paranawithana N, Zhang S, Lo ST, Wen X, Zhao P, Neeman M, Sherry AD. J Am Chem Soc. 2018; 140:17456–17464. [PubMed: 30484648]

25. De Leon-Rodriguez L, Josue A, Lubag M, Sherry AD. Inorganica Chim Acta. 2012; 393:12–23. [PubMed: 23180883]

26. Yu J, Martins AF, Preihs C, Clavijo Jordan V, Chirayil S, Zhao P, Wu Y, Nasr K, Kiefer GE, Sherry AD. J Am Chem Soc. 2015; 137:14173–14179. [PubMed: 26462412]

27. Miller LJ, Sexton PM, Dong M, Harikumar KG. Int J Obes Suppl. 2014; 4:S9–S13. [PubMed: 27152167]

28. Mikkola K, Bin Yim C, Fagerholm V, Ishizu T, Elomaa VV, Rajander J, Jurttila J, Saanijoki T, Tolvanen T, Tirri M, Gourni E, Béhé M, Gotthardt M, Reubi JC, Mäcke H, Roivainen A, Solin O, Nuutila P. Mol Imaging Biol. 2014; 16:255–263. [PubMed: 24101374]

29. Abe H, Uchida T, Hara A, Mizukami H, Komiya K, Koike M, Shigihara N, Toyofuku Y, Ogihara T, Uchiyama Y, Yagihashi S, Fujitani Y, Watada H. Endocrinology. 2013; 154:4512–4524. [PubMed: 24105478]

30. Werner U, Haschke G, Herling AW, Kramer W. Regul Pept. 2010; 164:58–64. [PubMed: 20570597]

31. Adriaenssens AE, Svendsen B, Lam BYH, Yeo GSH, Holst JJ, Reimann F, Gribble FM. Diabetologia. 2016; 59:2156–2165. [PubMed: 27390011]

32. Seino Y, Fukushima M, Yabe D. J Diabetes Invest. 2010; 1:8–23.

33. Raufman JP. Regul Pept. 1996; 61:1–18. [PubMed: 8701022]

34. Pfeffer MA, Claggett B, Diaz R, Dickstein K, Gerstein HC, Køber LV, Lawson FC, Ping L, Wei X, Lewis EF, Maggioni AP, McMurray JJV, Probstfield JL, Riddle MC, Solomon SD, Tardif J-C. N Engl J Med. 2015; 373:2247–2257. [PubMed: 26630143]

35. Parkes D, Jodka C, Smith P, Nayak S, Rinehart L, Gingerich R, Chen K, Young A. Drug Dev Res. 2001; 53:260–267.

36. Wang Q, Brubaker P. Diabetologia. 2002; 45:1263–1273. [PubMed: 12242459]

37. Farilla L, Hui H, Bertolotto C, Kang E, Bulotta A, Di Mario U, Perfetti R. Endocrinology. 2002; 143:4397–4408. [PubMed: 12399437]

38. Vinet L, Lamprianou S, Babic A, Lange N, Thorel F, Herrera PL, Montet X, Meda P. Diabetologia. 2014; 58:304–312. [PubMed: 25413047]

39. Wang P, Yoo B, Yang J, Zhang X, Ross A, Pantazopoulos P, Dai G, Moore A. Diabetes. 2014; 63:1465–1474. [PubMed: 24458362]

40. Luo Y, Pan Q, Yao S, Yu M, Wu W, Xue H, Kiesewetter DO, Zhu Z, Li F, Zhao Y, Chen X. J Nucl Med. 2016; 57:715–720. [PubMed: 26795291]

41. Kiesewetter DO, Gao H, Ma Y, Niu G, Quan Q, Guo N, Chen X. Eur J Nucl Med Mol Imaging. 2012; 39:463–473. [PubMed: 22170321]

42. Selvaraju RK, Velikyan I, Johansson L, Wu Z, Todorov I, Shively J, Kandeel F, Korsgren O, Eriksson O. J Nucl Med. 2013; 54:1458–1463. [PubMed: 23761918]

43. Brom M, Joosten L, Frielink C, Peeters H, Bos D, Van Zanten M, Boerman O, Gotthardt M. Diabetes. 2018; 67:2012–2018. [PubMed: 30045920]

44. Joosten L, Brom M, Peeters H, Bos D, Himpe E, Bouwens L, Boerman O, Gotthardt M. Mol Pharm. 2019; 16:4024–4030. [PubMed: 31345042]

45. Wild D, Wicki A, Mansi R, Behe M, Keil B, Bernhardt P, Christofori G, Ell PJ, Macke HR. J Nucl Med. 2010; 51:1059–1067. [PubMed: 20595511]

46. Sowa-Staszczak A, Trofimiuk-Müldner M, Stefanska A, Tomaszuk M, Buziak-Bereza M, Gilis-Januszewska A, Jabrocka-Hybel A, Glowa B, Malecki M, Bednarczuk T, Kaminski G, Kowalska A, Mikolajczak R, Janota B, Hubalewska-Dydejczyk A. PLoS One. 2016; 11:1–13.

47. Gotthardt M, Lalyko G, van Eerd-Vismale J, Keil B, Schurrat T, Hower M, Laverman P, Behr TM, Boerman OC, Göke B, Béhé M. Regul Pept. 2006; 137:162–167. [PubMed: 16930741]

48. Reiner T, Thurber G, Gaglia J, Vinegoni C, Liew CW, Upadhyay R, Kohler RH, Li L, Kulkarni RN, Benoist C, Mathis D, Weissleder R. Proc Natl Acad Sci. 2011; 108:12815–12820. [PubMed: 21768367]

49. Manandhar B, Ahn JM. J Med Chem. 2015; 58:1020–1037. [PubMed: 25349901]

50. Brand C, Abdel-Atti D, Zhang Y, Carlin S, Clardy SM, Keliher EJ, Weber WA, Lewis JS, Reiner T. Bioconjugate Chem. 2014; 25:1323–1330.

51. Eter WA, Van Der Kroon I, Andralojc K, Buitinga M, Willekens SMA, Frielink C, Bos D, Joosten L, Boerman OC, Brom M, Gotthardt M. Sci Rep.

52. Van Der Kroon I, Joosten L, Nock BA, Maina T, Boerman OC, Brom M, Gotthardt M. Mol Pharm. 2016; 13:3478–3483. [PubMed: 27537699]

53. Joosten L, Brom M, Peeters H, Heskamp S, Béhé M, Boerman O, Gotthardt M. Mol Pharm. 2018; 15:486–494. [PubMed: 29226686]

54. Senica K, Tomazic A, Skvarca A, Kolenc Peitl P, Mikolajczak R, Hubalewska-Dydejczyk A, Lezaic L. Mol Imaging Biol. 2020; 22:165–172. [PubMed: 31098984]

55. Carollo A, Papi S, Grana CM, Mansi L, Chinol M. Curr Radiopharm. 2019; 12:107–125. [PubMed: 30843499]

56. Pach D, Sowa-Staszczak A, Jabrocka-Hybel A, Stefanska A, Tomaszuk M, Mikolajczak R, Janota B, Trofimiuk-Müldner M, Przybylik-Mazurek E, Hubalewska-Dydejczyk A. Int J Endocrinol. 2013; 2013

57. Law, G-L, Wong, W-T. The Chemistry of Molecular Imaging. Long, NJ, Wong, W-T, editors. John Wiley & Sons; Hoboken, U.S.A: 2015. 1–24.

58. Clough TJ, Jiang L, Wong KL, Long NJ. Nat Commun. 2019

59. Aime S, Botta M, Crich SG, Giovenzana G, Pagliarin R, Sisti M, Terreno E. Magn Reson Chem. 1998; 36:S200–S208.

60. Garimella PD, Datta A, Romanini DW, Raymond KN, Francis MB. J Am Chem Soc. 2011; 133:14704–14709. [PubMed: 21800868]

61. Grobner T. Nephrol Dial Transpl. 2006; 21:1104–1108.

62. Aime S, Caravan P. J Magn Reson Imaging. 2009; 30:1259–1267. [PubMed: 19938038]

63. McDonald RJ, McDonald JS, Kallmes DF, Jentoft ME, Murray DL, Thielen KR, Williamson EE, Eckel LJ. Radiology. 2015; 275:772–782. [PubMed: 25742194]

64. Kanda T, Oba H, Toyoda K, Kitajima K, Furui S. Jpn J Radiol. 2016; 34:3–9. [PubMed: 26608061]

65. Gulani V, Calamante F, Shellock FG, Kanal E, Reeder SB. Lancet Neurol. 2017; 16:564–70. [PubMed: 28653648]

66. Dekkers IA, Roos R, Van Der Molen AJ. Eur Radiol. 2018; 28:1579–1584. [PubMed: 29063255]

67. Grobner T, Prischl FC. Kidney Int. 2007

68. Martinez-Sanchez A, Nguyen-Tu MS, Rutter GA. Mol Endocrinol. 2015; 29:1067–1079. [PubMed: 26038943]

69. Melkman-Zehavi T, Oren R, Kredo-Russo S, Shapira T, Mandelbaum AD, Rivkin N, Nir T, Lennox KA, Behlke MA, Dor Y, Hornstein E. EMBO J. 2011; 30:835–845. [PubMed: 21285947]

70. Savitzky A, Golay MJE. Anal Chem. 1964; 36:1627–1639.

71. Chen C, Cohrs CM, Stertmann J, Bozsak R, Speier S. Mol Metab. 2017; 6:943–957. [PubMed: 28951820]
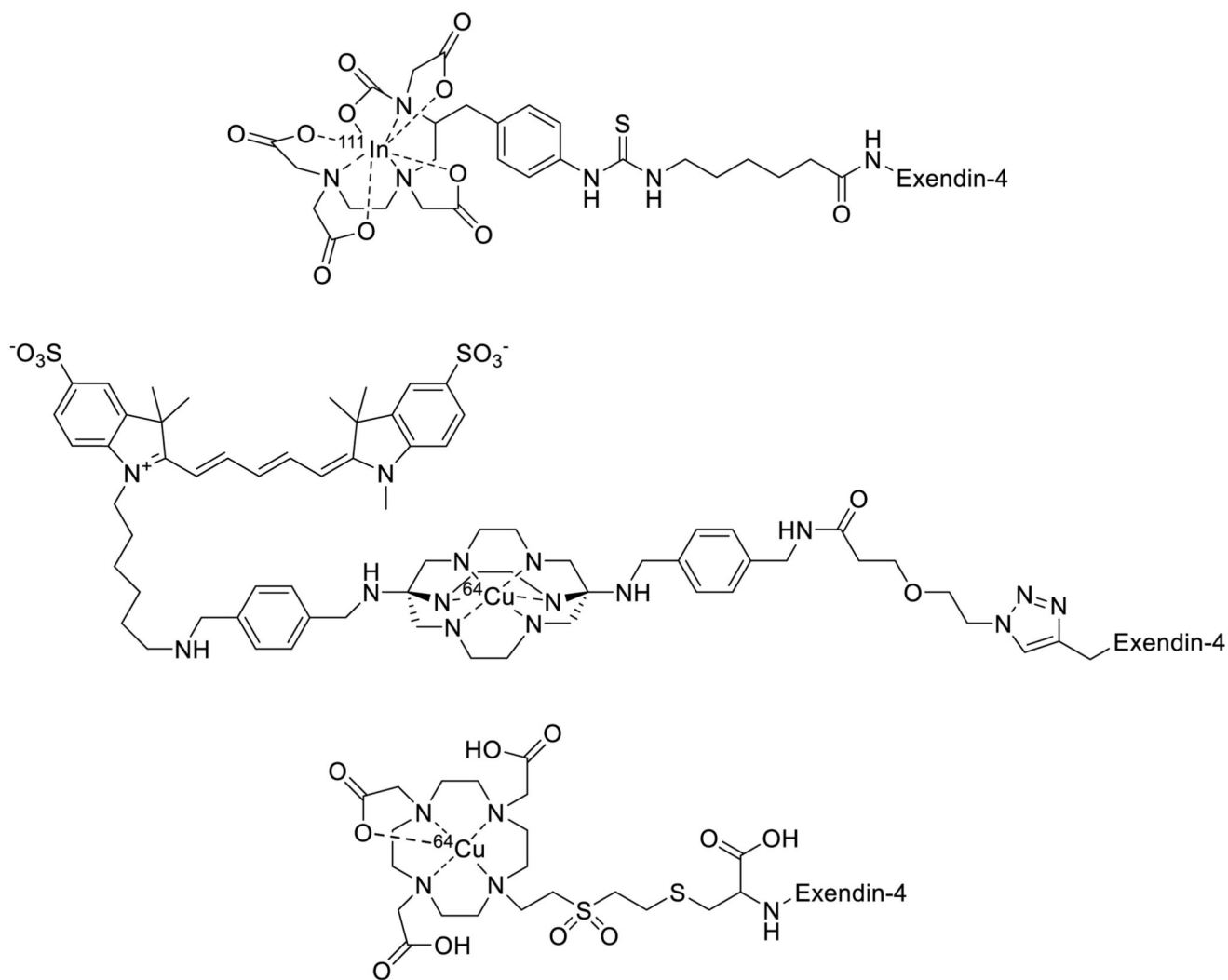
Figure 1.
Examples of the broad spectrum of exendin-4 conjugated imaging probes, with applications in SPECT, PET and fluorescence imaging[3,28,49,50].
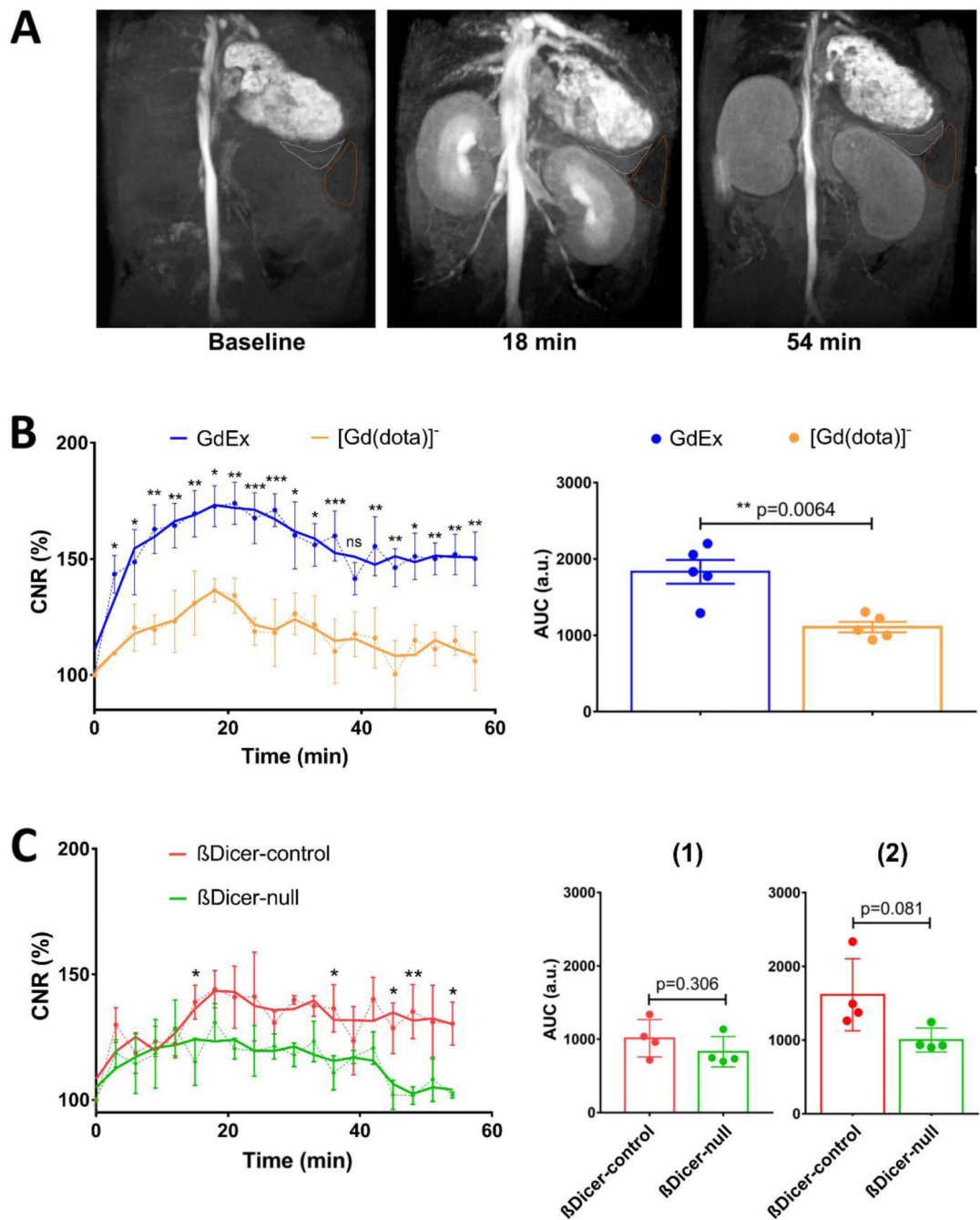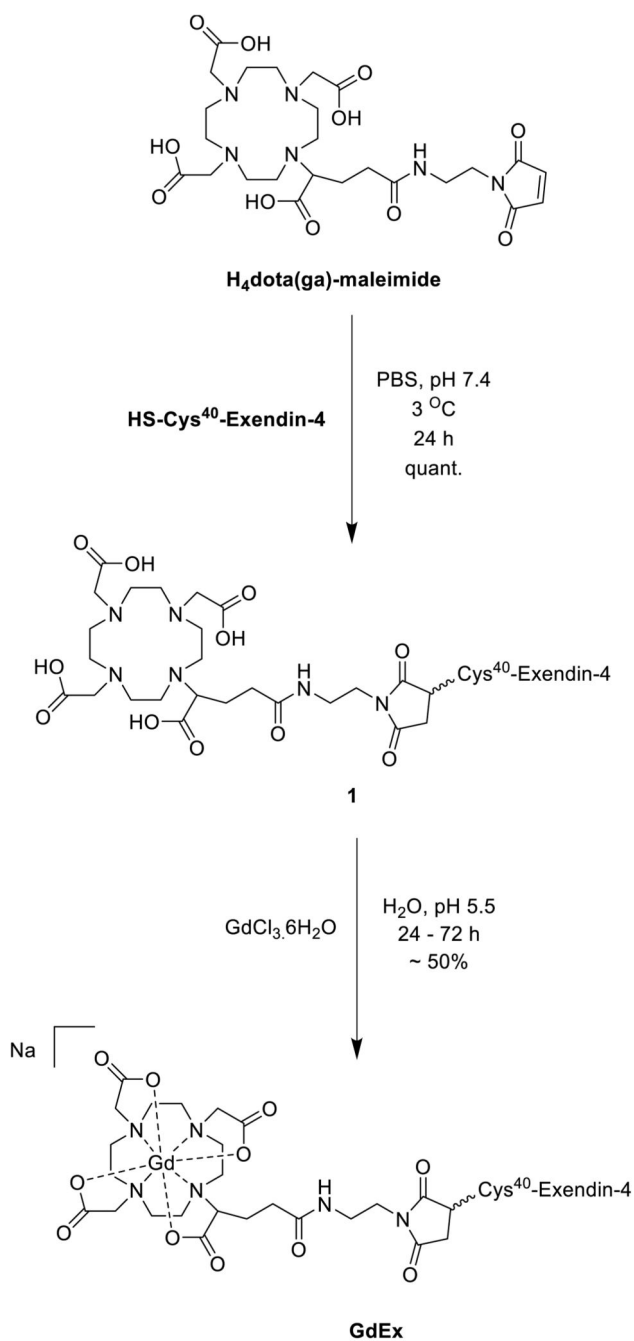
Figure 2.
A: Representative MRI of a healthy C57BL/6J mouse abdomen before (baseline), 18 min. and 54 min. after GdEx injection. Note the increased contrast of the pancreas relative to the baseline. The pancreas is outlined in white, spleen in brown. B, C: Time-course plot of (B) GdEx (blue) and [Gd(dota)]- (yellow) impact on the CNR of the pancreas in C57BL/6J mice and of (C) GdEx impact on the CNR of the pancreas of βDicer-null (green) and βDicer-control (red) mice. Data (mean ± S.E.M, n=5 animals/condition (B), n=4 animals/ phenotype) is presented as percentage (%) of CNR compared to baseline. The area under the

curve (AUC) is shown in the right-hand side panels spanning (B) the full time-course or (C) 0 to 21 min, (1) and 21 to 54 min. (2) after GdEx injection. Each dot represents AUC of a single mouse. *p<0.05, **p<0.01, ***p<0.001, two-way ANOVA (repeated measures), Fisher's LSD test (Time-courses), Student's t test (AUC) using GraphPad Prism 7.0.

H₄dota(ga)-maleimide

HS-Cys⁴⁰-Exendin-4

PBS, pH 7.4
3 °C
24 h
quant.

1

GdCl₃.6H₂O

H₂O, pH 5.5
24 - 72 h
~ 50%

GdEx

Scheme 1.
The synthesis of **GdEx**.